

Planar Hall effect in topological Weyl and nodal line semimetals

Lei Li,^{1,2} Jin Cao,^{1,2} Chaoxi Cui,^{1,2} Zhi-Ming Yu,^{1,2,*} and Yugui Yao^{1,2,†}

¹Centre for Quantum Physics, Key Laboratory of Advanced Optoelectronic Quantum Architecture and Measurement (MOE), School of Physics, Beijing Institute of Technology, Beijing, 100081, China

²Beijing Key Lab of Nanophotonics & Ultrafine Optoelectronic Systems, School of Physics, Beijing Institute of Technology, Beijing, 100081, China

Using symmetry analysis and semiclassical Boltzmann equation, we theoretically explore the planar Hall effect (PHE) in three-dimensional materials. We demonstrate that PHE is a general phenomenon that can occur in various systems regardless of band topology. Both the Lorentz force and Berry curvature effects can induce significant PHE, and the leading contributions of both effects linearly depend on the electric and magnetic fields. The Lorentz force and Berry curvature PHE coefficient possess only antisymmetric and symmetric parts, respectively. Both contributions respect the same crystalline symmetry constraints but differ under time-reversal symmetry. Remarkably, for topological Weyl semimetal, the Berry curvature PHE coefficient is a constant that does not depend on the Fermi energy, while the Lorentz force contribution linearly increases with the Fermi energy, resulting from the linear dispersion of the Weyl point. Furthermore, we find that the PHE in topological nodal line semimetals is mainly induced by the Lorentz force, as the Berry curvature in these systems vanishes near the nodal line. Our study not only highlights the significance of the Lorentz force in PHE, but also reveals its unique characteristics, which will be beneficial for determining the Lorentz force contribution experimentally.

I. INTRODUCTION

The study of magnetotransport has always attracted extensive attention in condensed matter physics. Due to the Lorentz force, electrons experience transverse force perpendicular to their moving direction under a magnetic field. Hence, for the systems with crossed electric and magnetic fields, it is easy to expect that there will exist a transverse current perpendicular to both electric and magnetic fields, known as the ordinary Hall effect [1, 2]. Besides, there are several other related phenomena, such as the anomalous Hall effect, spin Hall effect, and quantum (spin) Hall effect [3–7]. All of these Hall effects are crucial for both theoretical investigations and practical applications [3–10].

Interestingly, it has been discovered that a coplanar magnetic field and electric field can also induce a significant transverse current [11–14]. Since the exerted electric field, magnetic field, and Hall current all lie in the same plane, this phenomenon is called as planar Hall effect (PHE) [11–25]. Compared to the ordinary Hall effect, it generally is difficult to develop an intuitive picture to understand the PHE. Pal *et al.* [26] investigated the longitudinal magnetoresistance induced by the Lorentz force and showed that certain kinds of anisotropic spectrum may be relevant to the PHE.

In the past decade, with the discovery of graphene and topological Weyl semimetal, the field of topological materials has undergone rapid development [27–29]. Besides the Weyl and Dirac points, the conduction and valence bands of crystals can form many different kinds of degeneracies around the Fermi energy, such as triple

point, nodal line, and nodal surface [30–38]. Around these degeneracies, the electronic band generally exhibits significant Berry curvature and non-trivial band topology [28, 29], leading to various exotic properties [39–50]. The Berry curvature also has an important influence on the transport properties of systems [2]. Nandy *et al.* [51] have shown that the PHE can naturally appear in Weyl semimetals as a result of chiral anomaly, with the PHE conductivity depending quadratically on the magnetic field. This quadratic behavior has also been reported in many other works while with different origins [52, 53]. However, in the regime of strong B field, the chiral anomaly can lead to a linear dependence of the PHE on the field [54, 55]. Besides, for the systems with lower symmetry, such as anisotropic Weyl cone, the PHE conductivity also scales with the first order of magnetic field [56–58]. The PHE has been experimentally observed in many topological semimetals, such as PbTe_2 , ZrTe_5 , VAl_3 and WTe_2 [59–71]. However, there remains a lack of systematic investigation to show under which condition the PHE can or cannot occur. Besides, current research on PHE is generally based on Weyl semimetals and certain topological insulators [51, 53, 56–58, 72–78]. In contrast, the nodal line naturally exhibits strong anisotropic spectrum [35], suggesting that for PHE, the Lorentz force may play a more important role in nodal line systems than that in Weyl semimetals.

In this work, we perform a systematic symmetry analysis of the PHE conductivity, and show that linear PHE can exist in various systems with and without band topology. Then via the semiclassical Boltzmann equation, we expand the PHE conductivity to the linear order of the magnetic field, and find that both the Lorentz force and Berry curvature can cause linear PHE. Particularly, the Berry curvature contribution to linear PHE vanishes when the systems have time-reversal symmetry (\mathcal{T}). This

* zhiming_yu@bit.edu.cn

† ygyao@bit.edu.cn

TABLE I. The constraints on χ_{yx}^{even} and χ_{yx}^{odd} for some representative symmetry operations. “ \checkmark ” (“ \times ”) means the element is symmetry allowed (forbidden) by the operation.

	\mathcal{T}	\mathcal{P}	\mathcal{PT}	\mathcal{C}_{2x}	\mathcal{C}_{2y}	\mathcal{C}_{2z}	\mathcal{M}_x	\mathcal{M}_y	\mathcal{M}_z	\mathcal{C}_{3z}	\mathcal{C}_{4z}	\mathcal{C}_{6z}	\mathcal{S}_{3z}	\mathcal{S}_{4z}	\mathcal{S}_{6z}
$\chi_{yx,x}^{\text{odd}}$	\times	\checkmark	\times	\times	\checkmark	\times	\times	\checkmark	\times	\checkmark	\times	\times	\times	\times	\checkmark
$\chi_{yx,x}^{\text{even}}$	\checkmark	\checkmark	\checkmark	\times	\checkmark	\times	\times	\checkmark	\times	\checkmark	\times	\times	\times	\times	\checkmark
$\chi_{yx,y}^{\text{odd}}$	\times	\checkmark	\times	\checkmark	\times	\times	\checkmark	\times	\times	\checkmark	\times	\times	\times	\times	\checkmark
$\chi_{yx,y}^{\text{even}}$	\checkmark	\checkmark	\checkmark	\checkmark	\times	\times	\checkmark	\times	\times	\checkmark	\times	\times	\times	\times	\checkmark

means that even in topological semimetals, the Lorentz force may dominate linear PHE, as long as the system has \mathcal{T} symmetry. For general cases, both Berry curvature and Lorentz force contribute to PHE. We find that for the Weyl point, the Berry curvature (Lorentz force) contribution dominates linear PHE when the Fermi energy is close to (far from) the Weyl point, as the former is a constant that does not depend on the Fermi energy, while the latter linearly increases with the Fermi energy. However, for the nodal line systems, the Lorentz force contribution always dominates the linear PHE regardless of the position of Fermi level. Our results provide important insights into the PHE in topological semimetals, and are ready for experimental examination.

The paper is organized as follows. In Sec. II, we provide a systematic symmetry analysis of the PHE conductivity and summarize all the results in a table. In Sec. III, we derive the expressions for PHE conductivity based on the semiclassical Boltzmann transport theory. The specific numerical calculations of different models are described in Sec. IV. Finally, Sec. V contains a brief summary and discussion.

II. GENERAL ANALYSIS

Without loss of generality, we assume that the exerted electric field E , magnetic field B and Hall current all lie in the x - y plane, and the x axis aligns with the electric field direction. According to the linear response theory, the PHE conductivity σ_{yx} is obtained by [79]

$$j_y = \sigma_{yx}(B_x, B_y)E_x, \quad (1)$$

where j_y is the Hall current density, and $B_x = B \cos \theta$ and $B_y = B \sin \theta$ with θ denoting the angle between x axis and B field. When the magnetic field is weak, we can expand $\sigma_{yx}(B_x, B_y)$ in the powers of $B_{x(y)}$. Up to the linear order, $\sigma_{yx}(B_x, B_y)$ can be approximately written as

$$\sigma_{yx} = \sigma_{yx}^0 + \chi_{yx} \cdot \mathbf{B} \equiv \sigma_{yx}^0 + \chi_{yx,x} B_x + \chi_{yx,y} B_y. \quad (2)$$

σ_{yx}^0 has no dependence on B , resulting from the classical Drude conductivity and intrinsic anomalous Hall conductivity, while $\chi_{yx} \cdot \mathbf{B}$ corresponds to the magnetoconductivity induced by the magnetic field. Generally,

the coefficient χ_{yx} in Eq. (2) is a function of the relaxation time τ . Hence, we can further divide it into two parts,

$$\chi_{yx} = \chi_{yx}^{\text{even}} + \chi_{yx}^{\text{odd}}, \quad (3)$$

where χ_{yx}^{even} (χ_{yx}^{odd}) is an even (odd) function of τ . Then, the PHE conductivity can be rewritten as

$$\sigma_{yx} = \sigma_{yx}^0 + \sigma_{yx}^{\text{even}} + \sigma_{yx}^{\text{odd}}, \quad (4)$$

with $\sigma_{yx}^{\text{even}} = \chi_{yx}^{\text{even}} \cdot \mathbf{B}$ and $\sigma_{yx}^{\text{odd}} = \chi_{yx}^{\text{odd}} \cdot \mathbf{B}$.

The expressions of χ_{yx}^{even} and χ_{yx}^{odd} should respect the magnetic point group symmetry of systems. It should be stressed that the relaxation time τ in χ_{yx} reverses its sign under \mathcal{T} symmetry and the magnetic symmetry operators \mathcal{OT} with \mathcal{O} a spatial operator [42, 79]. We summarize the behaviors of $\chi_{yx}^{\text{even(odd)}}$ under different symmetry operations in Table I. One finds that χ_{yx}^{even} and χ_{yx}^{odd} respect the same spatial symmetry constraints, and only a few spatial operations like \mathcal{C}_{2z} and \mathcal{M}_z can completely suppress them (Notice that $\mathcal{C}_{4z}^2 = \mathcal{C}_{6z}^3 = \mathcal{S}_{4z}^2 = \mathcal{C}_{2z}$ and $\mathcal{S}_{3z}^3 = (\mathcal{C}_{6z}\mathcal{P})^3 = \mathcal{M}_z$). In addition, χ_{yx}^{odd} vanishes in the nonmagnetic systems. Because the symmetry analysis is irrelevant to the band topology, the results in Table I clearly show that the PHE can be realized in a wide variety of systems regardless of the band topology.

III. SEMICLASSICAL THEORY OF PHE CONDUCTIVITY

We then study the microscopic origin of the PHE conductivity σ_{yx} based on the semiclassical Boltzmann transport theory. In the presence of Berry curvature, the Bloch electrons under weak electric and magnetic fields can be described by the following semiclassical equations of motion [2, 80],

$$\dot{\mathbf{r}} = D(\mathbf{B}, \mathbf{\Omega}_{\mathbf{k}}) \left[\tilde{\mathbf{v}} + \frac{e}{\hbar} \mathbf{E} \times \mathbf{\Omega}_{\mathbf{k}} + \frac{e}{\hbar} (\tilde{\mathbf{v}} \cdot \mathbf{\Omega}_{\mathbf{k}}) \mathbf{B} \right], \quad (5)$$

$$\dot{\mathbf{k}} = D(\mathbf{B}, \mathbf{\Omega}_{\mathbf{k}}) \left[-\frac{e}{\hbar} \mathbf{E} - \frac{e}{\hbar} \tilde{\mathbf{v}} \times \mathbf{B} - \frac{e^2}{\hbar^2} (\mathbf{E} \cdot \mathbf{B}) \mathbf{\Omega}_{\mathbf{k}} \right], \quad (6)$$

where $\dot{\mathbf{r}}$ and $\dot{\mathbf{k}}$ are the time derivatives of position \mathbf{r} and wave vector \mathbf{k} , $D(\mathbf{B}, \mathbf{\Omega}_{\mathbf{k}}) \equiv [1 + e(\mathbf{B} \cdot \mathbf{\Omega}_{\mathbf{k}})/\hbar]^{-1}$

is the modification of phase space volume, $\mathbf{\Omega}_k = -2\epsilon_{\alpha\beta\gamma}\text{Im}\langle\partial_{k_\alpha}u(\mathbf{k})|\partial_{k_\beta}u(\mathbf{k})\rangle$ denotes the Berry curvature with $\epsilon_{\alpha\beta\gamma}$ the Levi-Civita tensor, $u(\mathbf{k})$ the cell-periodic part of Bloch function, and $\mathbf{v} = \partial_{\mathbf{k}}\tilde{\epsilon}/\hbar$ is the velocity of electrons. $\tilde{\epsilon}(\mathbf{k}) = \epsilon(\mathbf{k}) - \mathbf{m} \cdot \mathbf{B}$, $\epsilon(\mathbf{k})$ is the band dispersion and \mathbf{m} is the orbital magnetic moment results from the semiclassical self-rotation of the electron wave packet [2]. The electron charge is taken as $-e$ (i.e., $e > 0$).

The current density is given by [1, 2]

$$\mathbf{J} = -e \int \frac{d^3k}{(2\pi)^3} D^{-1} \dot{\mathbf{r}} f_{\mathbf{k}}(\mathbf{r}, t), \quad (7)$$

with $f_{\mathbf{k}}(\mathbf{r}, t)$ the distribution function, which can be determined by solving the semiclassical Boltzmann transport equation,

$$\frac{\partial f_{\mathbf{k}}}{\partial t} + \dot{\mathbf{r}} \cdot \frac{\partial f_{\mathbf{k}}}{\partial \mathbf{r}} + \dot{\mathbf{k}} \cdot \frac{\partial f_{\mathbf{k}}}{\partial \mathbf{k}} = \left(\frac{\partial f_{\mathbf{k}}}{\partial t} \right)_{\text{coll}}. \quad (8)$$

The right side of Eq. (8) is known as the collision integral and generally can be treated by relaxation time approximation [1]. Then, for a homogeneous system in the steady state, where $\partial f/\partial t$ and $\partial f/\partial \mathbf{r}$ vanish, Eq. (8) is simplified as

$$\dot{\mathbf{k}} \cdot \frac{\partial f_{\mathbf{k}}}{\partial \mathbf{k}} = -\frac{f_{\mathbf{k}} - f_{\mathbf{k}}^0}{\tau} \equiv -\frac{g_{\mathbf{k}}}{\tau}, \quad (9)$$

with $f_{\mathbf{k}}^0$ the original Fermi-Dirac distribution function and τ the relaxation time. In the following calculations, we take the relaxation time τ as 0.1 ps [51, 81–83]. Notice that $g_{\mathbf{k}}$ vanishes when $E = 0$. Hence, for a weak E field, we can approximately assume $g_{\mathbf{k}} = \mathbf{\Gamma} \cdot \mathbf{E}$, where $\mathbf{\Gamma}$ is a function to be determined. Substituting the expression of $g_{\mathbf{k}}$ into Eq. (9), and keeping only the linear order of \mathbf{E} and \mathbf{B} (as well as their combination $E_i B_j$), $\mathbf{\Gamma}$ and the distribution function $f_{\mathbf{k}}$ can be determined. Then, the expression of current density is obtained as

$$\begin{aligned} \mathbf{J} &= e^2 \int [d\mathbf{k}] [\tau \hbar \mathbf{v}(\mathbf{v} \cdot \mathbf{E}) \partial_{\epsilon} f_{\mathbf{k}}^0 - (\mathbf{E} \times \mathbf{\Omega}_k) f_{\mathbf{k}}^0] \\ &- e^2 \tau \int [d\mathbf{k}] [\mathbf{v}(\partial_{\mathbf{k}}(\mathbf{m} \cdot \mathbf{B}) \cdot \mathbf{E}) + (\mathbf{v} \cdot \mathbf{E}) \partial_{\mathbf{k}}(\mathbf{m} \cdot \mathbf{B})] \partial_{\epsilon} f_{\mathbf{k}}^0 \\ &- e^3 \tau \int [d\mathbf{k}] \mathbf{v}(\mathbf{v} \cdot \mathbf{E})(\mathbf{B} \cdot \mathbf{\Omega}_k) \partial_{\epsilon} f_{\mathbf{k}}^0 \\ &+ e^3 \tau \int [d\mathbf{k}] [\mathbf{B}(\mathbf{v} \cdot \mathbf{E}) + \mathbf{v}(\mathbf{B} \cdot \mathbf{E})] (\mathbf{v} \cdot \mathbf{\Omega}_k) \partial_{\epsilon} f_{\mathbf{k}}^0 \\ &+ e^3 \tau^2 \int [d\mathbf{k}] \mathbf{v}[(\mathbf{v} \times \mathbf{B}) \cdot \partial_{\mathbf{k}}(\mathbf{v} \cdot \mathbf{E})] \partial_{\epsilon} f_{\mathbf{k}}^0, \end{aligned} \quad (10)$$

with $\int [d\mathbf{k}] \equiv -\frac{1}{(2\pi)^3 \hbar} \int d^3k$ and $\mathbf{v} = \partial_{\mathbf{k}}\epsilon/\hbar$. This result is consistent with the previous works [26, 56] but it captures all the terms up to order $O(E)$ and $O(EB)$. Consequently, the expressions of the PHE conductivity $\sigma_{yx} = \sigma_{yx}^0 + \sigma_{yx}^{\text{even}} + \sigma_{yx}^{\text{odd}}$ are

$$\sigma_{yx}^0 = e^2 \int [d\mathbf{k}] (\tau \hbar v_x v_y \frac{\partial f_{\mathbf{k}}^0}{\partial \epsilon} - \Omega_k^z f_{\mathbf{k}}^0), \quad (11)$$

which are the classical Drude conductivity and intrinsic anomalous Hall conductivity, and

$$\begin{aligned} \sigma_{yx}^{\text{even}} &= e^3 \tau^2 \int [d\mathbf{k}] \frac{\partial f_{\mathbf{k}}^0}{\partial \epsilon} v_y (\mathbf{v} \times \mathbf{B}) \cdot \frac{\partial v_x}{\partial \mathbf{k}}, \quad (12) \\ \sigma_{yx}^{\text{odd}} &= e^3 \tau \int [d\mathbf{k}] \frac{\partial f_{\mathbf{k}}^0}{\partial \epsilon} \left[-(\mathbf{B} \cdot \mathbf{\Omega}_k) v_x v_y \right. \\ &\quad \left. - \frac{v_y}{e} \partial_{k_x}(\mathbf{m} \cdot \mathbf{B}) - \frac{v_x}{e} \partial_{k_y}(\mathbf{m} \cdot \mathbf{B}) \right. \\ &\quad \left. + (B_x v_y + B_y v_x)(\mathbf{v} \cdot \mathbf{\Omega}_k) \right]. \end{aligned} \quad (13)$$

Clearly, σ_{yx}^{odd} is induced by the Berry curvature and is an odd function of τ , as it is in direct proportion to τ . In contrast, $\sigma_{yx}^{\text{even}}$ describes the Lorentz force contribution to PHE conductivity and is an even function of τ . This means that under \mathcal{T} symmetry, $\sigma_{yx}^{\text{even}}$ is invariant while σ_{yx}^{odd} should reverse its sign. Hence, for the systems with \mathcal{T} symmetry, σ_{yx}^{odd} vanishes and the leading order of the Berry curvature contribution to PHE is quadratic. Remarkably, we find that σ_{yx}^{odd} is symmetric in its two indices, namely $\sigma_{yx}^{\text{odd}} = \sigma_{xy}^{\text{odd}}$. Moreover, both σ_{yx}^{odd} and $\sigma_{yx}^{\text{even}}$ have the term of $\partial f_{\mathbf{k}}^0/\partial \epsilon$, indicating that only the electronic states around the Fermi level have contribution to them.

IV. MODEL STUDIES

A. Single-band model

To unambiguously demonstrate that the PHE can be induced by Lorentz force, we investigate a single-band model, where the Berry curvature is definitely zero. Consider a simple model that meets the symmetry requirements listed in Table I, for which the Hamiltonian can be written as

$$\mathcal{H}_1 = \frac{k^2}{2m} + A k_x k_z, \quad (14)$$

where $k^2 = k_x^2 + k_y^2 + k_z^2$, m is the effective mass of electron and the parameter A is a real number, denoting the anisotropy of the system [see Fig. 1(a)]. One can check that the model (14) breaks the \mathcal{C}_{2z} symmetry when A is finite. Hence, PHE can (not) be realized in it when $A \neq 0$ ($A = 0$). As shown in Fig. 1(b), this extremely simple model indeed produces a significant PHE signal with an angular dependence proportional to $\cos \theta$. Since the anisotropy is a common feature in real materials, one can expect that PHE in most real materials can be significant and has a period of 2π by varying the direction of magnetic field in the x - y plane.

B. Weyl semimetals

Although the PHE in Weyl semimetals has been studied in previous works [51, 53, 56–58], here we focus on the

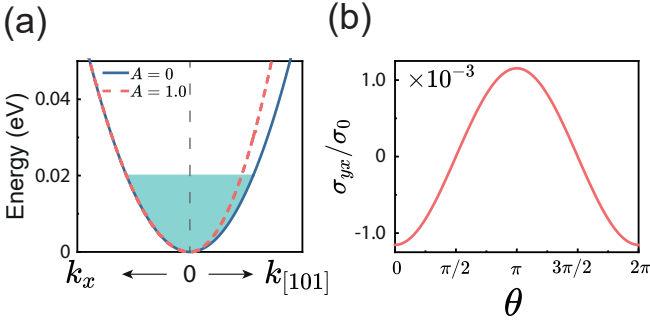


FIG. 1. (a) Energy spectrum of the single-band model (14) without (with) anisotropic effect. (b) Calculated PHC versus the angle θ for model (14), using Fermi level $E_F = 20$ meV and the magnetic field $B = 0.5$ T. In the calculations, we take the model parameter $m = 0.5$ eV $^{-1} \cdot \text{\AA}^{-2}$, $A = 1.0$ eV $\cdot \text{\AA}^2$ and the PHC is normalized by the corresponding longitudinal conductivity without magnetic field [i.e. $\sigma_0 = \sigma_{xx}(B = 0; E_F = 20$ meV)].

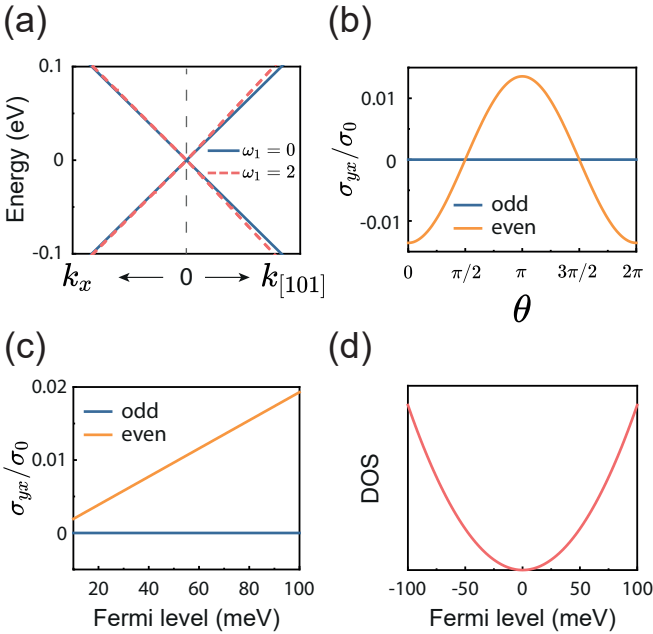


FIG. 2. (a) Band structure of Weyl model (15). (b) Calculated σ_{yx}^{odd} and $\sigma_{yx}^{\text{even}}$ as functions of angle θ , using $E_F = 50$ meV and $B = 0.05$ T. (c) Variation of σ_{yx}^{odd} and $\sigma_{yx}^{\text{even}}$ with Fermi level with $\theta = 3\pi/4$. (d) The density of states (DOS) of Weyl model (15). In the calculations, we take $\omega_1 = 2.0$ eV $\cdot \text{\AA}$, $v_1 = 12.0$ eV $\cdot \text{\AA}$ and the conductivities in (b) and (c) are normalized by $\sigma_0 = \sigma_{xx}(B = 0; E_F = 100$ meV).

competition between the Berry curvature and the Lorentz force contributions to PHE, and show under what conditions the Berry curvature or the Lorentz force contribution will dominate PHE. For ideal Weyl point described by $\mathbf{k} \cdot \boldsymbol{\sigma}$ ($\boldsymbol{\sigma}$ s are Pauli matrices), both σ_{yx}^{odd} and $\sigma_{yx}^{\text{even}}$ are zero, due to the high symmetry of this model. Consequently, the chiral anomaly contribution dominates PHE

in conventional topological Weyl semimetals, resulting in PHE having a quadratic dependence on the magnetic field and an angular dependence with a period of π [51].

Breaking C_{2z} but keeping \mathcal{T} symmetry leads to the vanishing of σ_{yx}^{odd} , while the Lorentz force contribution $\sigma_{yx}^{\text{even}}$ will appear and dominate the PHE in the limit of weak B -field. To demonstrate this directly, we consider the following Weyl Hamiltonian

$$\mathcal{H}_2 = w_1 k_x \sigma_z + v_1 \mathbf{k} \cdot \boldsymbol{\sigma}, \quad (15)$$

where w_1 and v_1 are real parameters. The energy dispersion of this two-band model is $\varepsilon_{\pm}(\mathbf{k}) = \pm \sqrt{k^2 v_1^2 + k_x^2 w_1^2 + 2k_x k_z v_1 w_1}$, where \pm denotes the conduction and valence bands, respectively. From the band structure shown in Fig. 2(a), one observes that the additional term $w_1 k_x \sigma_z$ increases the slope along [101] direction and changes the shape of the Fermi surface from a sphere to an ellipsoid.

The calculated results of PHE based on Hamiltonian \mathcal{H}_2 (15) are shown in Fig. 2. One observes that σ_{yx}^{odd} is always zero regardless of the direction of B -field as guaranteed by the \mathcal{T} symmetry, while $\sigma_{yx}^{\text{even}}$ is finite except $\mathbf{B} \perp \mathbf{E}$ and becomes largest when $\mathbf{B} \parallel \mathbf{E}$. The period of $\sigma_{yx}^{\text{even}}$ in θ is 2π . Since the density of state of the Weyl system (15) increases with the Fermi energy [Fig. 2(d)], one can expect that $\sigma_{yx}^{\text{even}}$ would become more and more significant by raising the Fermi energy. The calculated $\sigma_{yx}^{\text{even}}$ as a function of E_F is shown in Fig. 2(c), where a linear increase of $\sigma_{yx}^{\text{even}}$ is observed. This linear dependence of $\sigma_{yx}^{\text{even}}$ on E_F is guaranteed by the linear Hamiltonian of the Weyl system, and can be easily obtained by the scaling analysis proposed by Cao et. al. [84]. Specifically, let us consider a scaling transformation in momentum and energy: $\mathbf{k} \rightarrow \lambda \mathbf{k}$ and $E_F \rightarrow \lambda E_F$, where λ is a real number. Due to the linear Hamiltonian, one has $\mathcal{H}_2(\lambda \mathbf{k}) = \lambda \mathcal{H}_2(\mathbf{k})$ and $\varepsilon(\lambda \mathbf{k}) = \lambda \varepsilon(\mathbf{k})$. However, the velocity and the eigenstates of system are invariant under the scaling, i.e. $v(\lambda \mathbf{k}) = v(\mathbf{k})$ and $|u_{n,\lambda \mathbf{k}}\rangle = |u_{n,\mathbf{k}}\rangle$. Thus, for Eq. (12), we find that $\sigma_{yx}^{\text{even}}(\lambda E_F) = \lambda \sigma_{yx}^{\text{even}}(E_F)$, indicating $\sigma_{yx}^{\text{even}}(E_F) \propto E_F$.

When both C_{2z} and \mathcal{T} symmetries of systems are broken, σ_{yx}^{odd} and $\sigma_{yx}^{\text{even}}$ become finite. However, because the Berry curvature is significantly reduced by increasing Fermi energy in Weyl semimetals, it can be expected that σ_{yx}^{odd} would not linearly increase with the Fermi energy. In fact, according to the aforementioned scaling analysis, one can find that $\sigma_{yx}^{\text{odd}}(\lambda E_F) = \sigma_{yx}^{\text{odd}}(E_F)$ due to $\boldsymbol{\Omega}_{\lambda \mathbf{k}} = \lambda^{-2} \boldsymbol{\Omega}_{\mathbf{k}}$ and $\mathbf{m}_{\lambda \mathbf{k}} = \lambda^{-1} \mathbf{m}_{\mathbf{k}}$. Hence, the σ_{yx}^{odd} is a constant that does not depend on E_F . Thus, the competition between σ_{yx}^{odd} and $\sigma_{yx}^{\text{even}}$ may lead a sign reversal of the total PHC conductivity by increasing the E_F .

The Weyl Hamiltonian breaking C_{2z} and \mathcal{T} may be written as

$$\mathcal{H}_3 = w_2 k_x + w_1 k_x \sigma_z + v_1 \mathbf{k} \cdot \boldsymbol{\sigma}, \quad (16)$$

where the additional term $w_2 k_x$ breaks \mathcal{T} symmetry. For this Weyl model, we numerically evaluate σ_{yx}^{odd} and $\sigma_{yx}^{\text{even}}$

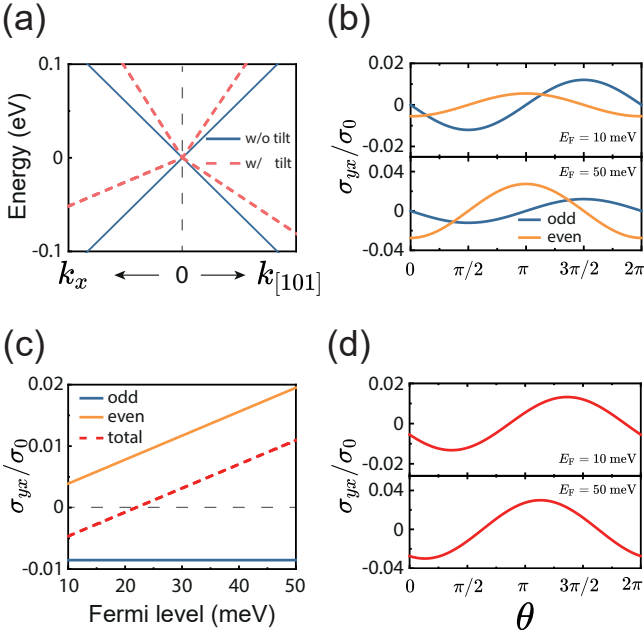


FIG. 3. (a) Band structure of Weyl model (16) without (with) tilt term. (b) The competition between σ_{yx}^{odd} and $\sigma_{yx}^{\text{even}}$ under different Fermi level. (c) Variation of σ_{yx}^{odd} , $\sigma_{yx}^{\text{even}}$ and the total PHC $\sigma_{yx}^{\text{total}}$ with Fermi level for $\theta = 3\pi/4$. (d) The calculated total PHC versus angle θ with $E_F = 10$ and 50 meV. In the calculations, we take magnetic field $B = 0.05$ T, model parameter $\omega_1 = 1.0$ eV \cdot \AA , $\omega_2 = 7.0$ eV \cdot \AA , $v_1 = 12.0$ eV \cdot \AA and the conductivities in (b), (c) and (d) are normalized by $\sigma_0 = \sigma_{xx}(B = 0; E_F = 50$ meV).

as functions of θ and E_F , and the obtained results are plotted in Fig. 3. Again, σ_{yx}^{odd} and $\sigma_{yx}^{\text{even}}$ vary with the direction of B -field in the period of 2π due to the linear dependence on B . Remarkably, we find that for electron doping ($E_F > 0$), the $\sigma_{yx}^{\text{even}}$ is always positive and linearly increases with E_F , while σ_{yx}^{odd} is a negative constant. Thus, the total PHE conductivity is negative for small E_F but changes its sign when E_F becomes large. This sign change of the total PHE may be detected in experiments.

C. Nodal line semimetals

At last, we study the PHE in topological nodal line semimetals. Numbers of real materials have been predicted to be topological nodal line semimetals, and most of them exhibit \mathcal{T} symmetry [37, 85–90]. With the above symmetry analysis, we know that in these nonmagnetic nodal line semimetals, the PHE is mainly induced by the Lorentz force when the fields are weak. Moreover, for the nodal line protected by \mathcal{PT} symmetry (\mathcal{P} is the spatial inversion symmetry), the Lorentz force contribution also dominates the PHE, as \mathcal{PT} symmetry guarantees the Berry curvature of systems to vanish.

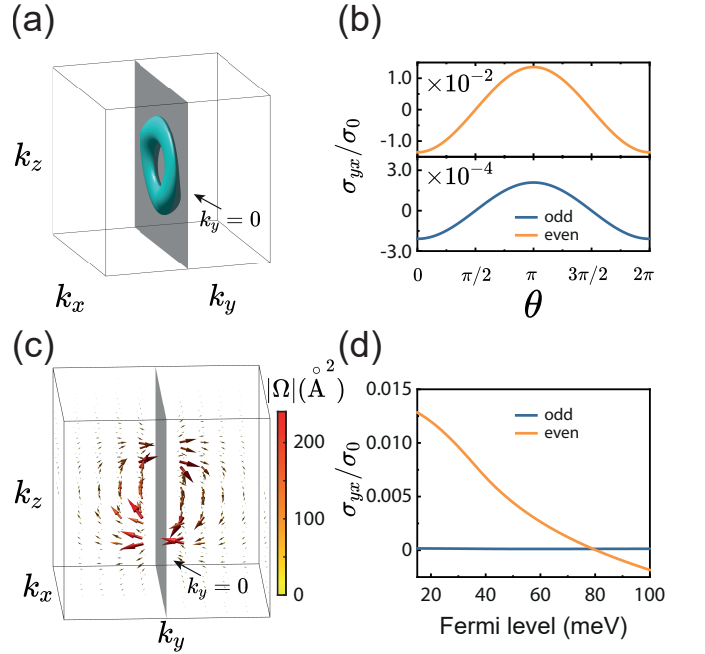


FIG. 4. (a) Side view of model (17)'s the Fermi surface. (b) The normalized σ_{yx}^{odd} and $\sigma_{yx}^{\text{even}}$ as functions of angle θ . (c) The Berry curvature distribution of the nodal line model (17) in the Brillouin zone (BZ). (d) Variation of σ_{yx}^{odd} and $\sigma_{yx}^{\text{even}}$ with Fermi level for $\theta = 3\pi/4$. σ_{yx}^{odd} is several orders of magnitude smaller than $\sigma_{yx}^{\text{even}}$. In (a) and (b), we take Fermi level $E_F = 30$ meV. In all calculations, we take $B = 0.5$ T, $c = 1.0$ eV \cdot \AA^2 , $m_0 = 0.04$ eV, $m_1 = 5.0$ eV \cdot \AA^2 , $v_y = 0.9$ eV \cdot \AA , $\omega_1 = \omega_2 = 14.0$ eV \cdot \AA^2 , $\omega_3 = 30.0$ eV \cdot \AA^2 and the conductivities in (b) and (d) are normalized by $\sigma_0 = \sigma_{xx}(B = 0; E_F = 30$ meV).

Here, we consider a nodal line model that breaks both \mathcal{T} and \mathcal{PT} symmetries to explore the competition between Berry curvature and Lorentz force effects. For a concrete example, we take a nodal line with a mirror symmetry \mathcal{M}_y , for which a general Hamiltonian may be written as

$$\mathcal{H}_4 = ck^2 + (m_0 - m_1k^2)\sigma_z + v_yk_y\sigma_y + (w_1k_x + w_2k_z + w_3k_x^2)k_y\sigma_x, \quad (17)$$

where $c, m_0, m_1, v_y, \omega_1, \omega_2$ and ω_3 are real parameters. When $m_0m_1 < 0$, we have a mirror-protected nodal line lying in the $k_y = 0$ plane, as shown in Fig. 4(a).

In sharp contrast to the Weyl semimetals, we find that the Berry curvature contribution to PHE (σ_{yx}^{odd}) in nodal line semimetals is several orders of magnitude smaller than the Lorentz force contribution ($\sigma_{yx}^{\text{even}}$), as shown in Fig. 4(b) and 4(d). Further calculations reveal that the strong suppression of the Berry curvature contribution can be attributed to the special distribution of the Berry curvature of the nodal line.

Generally, one can expect that the Berry curvature is significant around the band degeneracies, as it is inversely proportional to the square of band gap [2]. However, this

is not the case for the mirror-protected nodal line. Since the model (17) has \mathcal{M}_y symmetry and the nodal line resides in $k_y = 0$ plane, we study the distribution of the Berry curvature of this system in $k_y = 0$ plane. Because the Berry curvature $\mathbf{\Omega}(\mathbf{k})$ is a pseudovector, only the y -component of $\mathbf{\Omega}(\mathbf{k})$ can be nonzero in a \mathcal{M}_y -invariant plane. Hence, one has $\Omega_x = \Omega_z = 0$ in the $k_y = 0$ plane. To calculate $\Omega_y(k_y = 0)$, we consider a 2D system, for which the Hamiltonian is

$$\begin{aligned} H_{2D}(k_x, k_z) &= \mathcal{H}_4(k_x, k_y = 0, k_z) \\ &= ck_x^2 + ck_z^2 + (m_0 - m_1 k_x^2 - m_1 k_z^2)\sigma_z. \end{aligned} \quad (18)$$

A key feature of this 2D Hamiltonian is that the two bands in it are decoupled, indicating that the Berry curvature in this system must be zero, i.e. $\Omega_y(k_y = 0) = 0$. Therefore, while the nodal line may exhibit sizable Berry curvature in momentum space, it features vanishing rather than divergent Berry curvature around the band degeneracy, i.e. the nodal line [see Fig. 4(c)]. This is completely different from the case in Weyl point [28].

We also study the behaviors of σ_{yx}^{odd} and $\sigma_{yx}^{\text{even}}$ by varying E_F . As shown in Fig. 4(d), although the Berry curvature contribution increases with Fermi energy, it is always much smaller than the Lorentz force contribution. Another difference between Weyl points and nodal lines is that the Lorentz force contribution ($\sigma_{yx}^{\text{even}}$) in nodal line models may decrease when Fermi energy increases [see Fig. 4(d)], because the velocity of electrons around nodal line has a strong dependence on momentum and Fermi energy, and some of its components decrease when the Fermi energy increases.

Additionally, the nodal line is expected to exhibit strong direction-dependent transport behavior due to its highly anisotropic band dispersion. We rotate the nodal line by 90° around the z -axis and the rotated Fermi surface is depicted in Fig. 5(a). The calculated PHE conductivity σ_{yx} for this rotated nodal line is shown in Fig. 5(b). As expected, the σ_{yx} is still dominated by the contribution from the Lorentz force. The lower amplitude of $\sigma_{yx}^{\text{even}}$ in Fig. 5(b) is ascribed to the higher longitudinal conductivity $\sigma_{xx}(B = 0)$.

V. DISCUSSION AND CONCLUSION

In this work, we have studied the PHE in topological Weyl and nodal line semimetals. Both Lorentz force and Berry curvature contributions to PHE are discussed. We demonstrated that these two contributions respect the same crystalline symmetry constraints and are entirely suppressed by only a few symmetries. However, their responses to \mathcal{T} symmetry are opposite. Our results indicate that the PHE can occur in a wide variety of systems with and without band topology. Remarkably, we show the Lorentz force contribution can dominate the PHE in

various topological systems, including Weyl semimetals with \mathcal{T} symmetry and topological nodal line semimetals.

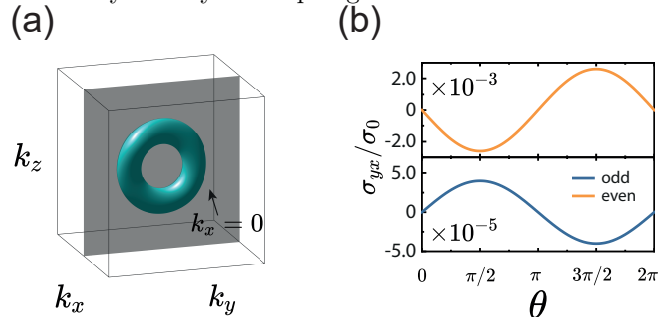


FIG. 5. (a) The side view of Fermi surface of rotated nodal line model (17) with $E_F = 30$ meV. (b) The normalized σ_{yx}^{odd} and $\sigma_{yx}^{\text{even}}$ as a function of angle θ . The parameter is taken the same as Fig. (4)

In experimentation, the angular dependence and the order of relaxation time in PHE can be directly examined using magnetotransport measurements [91, 92]. As discussed above, the Lorentz force PHE conductivity is directly proportional to \mathbf{B} and τ^2 , while the Berry curvature PHE conductivity (including the PHE conductivity induced by chiral anomaly) is proportional to the odd order of τ . Such unique behavior could be beneficial for experimentally identifying the Lorentz force contribution to PHE.

Generally, both the Lorentz force and the Berry curvature can also induce finite PHE in topological nodal surface semimetals, which is protected by the presence of a two-fold screw rotation and \mathcal{T} symmetry [33]. Compared with the Weyl points and the nodal lines, the anisotropy of the nodal surface is the strongest. Particularly, the topological charge of the nodal surface can be any integer depending on the material details [93, 94]. This means that the strength of the Berry curvature around the nodal surface can be tuned by model parameters. Hence, the competition between the Berry curvature and the Lorentz force contributions to PHE in the nodal surface would be interesting, and varies with the model of the nodal surface.

VI. ACKNOWLEDGEMENT

The authors thank J. Xun for helpful discussions. This work is supported by the NSF of China (Grants Nos. 12004035, 12234003 and 12061131002), the China Postdoctoral Science Foundation (Grants Nos. 2021TQ0043 and 2021M700437) and the National Natural Science Fund for Excellent Young Scientists Fund Program (Overseas).

-
- [1] N. W. Ashcroft and N. D. Mermin, *Solid state physics* (Holt, Rinehart and Winston, 1976).
- [2] D. Xiao, M.-C. Chang, and Q. Niu, Berry phase effects on electronic properties, *Rev. Mod. Phys.* **82**, 1959 (2010).
- [3] N. Nagaosa, J. Sinova, S. Onoda, A. H. MacDonald, and N. P. Ong, Anomalous Hall effect, *Rev. Mod. Phys.* **82**, 1539 (2010).
- [4] J. Sinova, S. O. Valenzuela, J. Wunderlich, C. H. Back, and T. Jungwirth, Spin Hall effects, *Rev. Mod. Phys.* **87**, 1213 (2015).
- [5] K. von Klitzing, Quantum Hall effect: Discovery and application, *Annual Review of Condensed Matter Physics* **8**, 13 (2017).
- [6] B. Huckestein, Scaling theory of the integer quantum Hall effect, *Rev. Mod. Phys.* **67**, 357 (1995).
- [7] B. A. Bernevig and S.-C. Zhang, Quantum spin Hall effect, *Phys. Rev. Lett.* **96**, 106802 (2006).
- [8] J. Lenz, A review of magnetic sensors, *Proceedings of the IEEE* **78**, 973 (1990).
- [9] J. Lenz and S. Edelstein, Magnetic sensors and their applications, *IEEE Sensors Journal* **6**, 631 (2006).
- [10] J. Daughton, GMR applications, *Journal of Magnetism and Magnetic Materials* **192**, 334 (1999).
- [11] B. Zhao, X. Yan, and A. B. Pakhomov, Anisotropic magnetoresistance and planar Hall effect in magnetic metal-insulator composite films, *Journal of Applied Physics* **81**, 5527 (1997).
- [12] A. Nemoto, Y. Otani, S. G. Kim, K. Fukamichi, O. Kitakami, and Y. Shimada, Magnetoresistance and planar Hall effects in submicron exchange-coupled NiO/Fe₁₉Ni₈₁ wires, *Applied Physics Letters* **74**, 4026 (1999).
- [13] H. X. Tang, R. K. Kawakami, D. D. Awschalom, and M. L. Roukes, Giant planar Hall effect in epitaxial (Ga,Mn)As devices, *Phys. Rev. Lett.* **90**, 107201 (2003).
- [14] M. Bowen, K.-J. Friedland, J. Herfort, H.-P. Schönherr, and K. H. Ploog, Order-driven contribution to the planar Hall effect in Fe₃Si thin films, *Phys. Rev. B* **71**, 172401 (2005).
- [15] K. M. Seemann, F. Freimuth, H. Zhang, S. Blügel, Y. Mokrousov, D. E. Bürgler, and C. M. Schneider, Origin of the planar Hall effect in nanocrystalline Co₆₀Fe₂₀B₂₀, *Phys. Rev. Lett.* **107**, 086603 (2011).
- [16] S.-H. Zheng, H.-J. Duan, J.-K. Wang, J.-Y. Li, M.-X. Deng, and R.-Q. Wang, Origin of planar Hall effect on the surface of topological insulators: Tilt of Dirac cone by an in-plane magnetic field, *Phys. Rev. B* **101**, 041408 (2020).
- [17] V. A. Zyuzin, In-plane Hall effect in two-dimensional helical electron systems, *Phys. Rev. B* **102**, 241105 (2020).
- [18] P. He, S. S.-L. Zhang, D. Zhu, S. Shi, O. G. Heinonen, G. Vignale, and H. Yang, Nonlinear planar Hall effect, *Phys. Rev. Lett.* **123**, 016801 (2019).
- [19] J. H. Cullen, P. Bhalla, E. Marcellina, A. R. Hamilton, and D. Culcer, Generating a topological anomalous Hall effect in a nonmagnetic conductor: An in-plane magnetic field as a direct probe of the Berry curvature, *Phys. Rev. Lett.* **126**, 256601 (2021).
- [20] L. Xiang and J. Wang, Intrinsic planar Hall effect in magnetic Weyl semimetals (2023), [arXiv:2209.03527](https://arxiv.org/abs/2209.03527) [cond-mat.mes-hall].
- [21] H. Wang, Y.-X. Huang, H. Liu, X. Feng, J. Zhu, W. Wu, C. Xiao, and S. A. Yang, Theory of intrinsic in-plane Hall effect (2022), [arXiv:2211.05978](https://arxiv.org/abs/2211.05978) [cond-mat.mes-hall].
- [22] Y. Wang, Z.-G. Zhu, and G. Su, Field-induced Berry connection and planar Hall effect in tilted Weyl semimetals (2023), [arXiv:2303.03579](https://arxiv.org/abs/2303.03579) [cond-mat.mes-hall].
- [23] Y.-W. Wei, J. Feng, and H. Weng, Spatial symmetry modulation of planar Hall effect in Weyl semimetals, *Phys. Rev. B* **107**, 075131 (2023).
- [24] Y.-X. Huang, X. Feng, H. Wang, C. Xiao, and S. A. Yang, Intrinsic nonlinear planar Hall effect, *Phys. Rev. Lett.* **130**, 126303 (2023).
- [25] J. Cao, W. Jiang, X.-P. Li, D. Tu, J. Zhou, J. Zhou, and Y. Yao, In-plane anomalous hall effect in pt-symmetric antiferromagnetic materials (2022), [arXiv:2208.14251](https://arxiv.org/abs/2208.14251) [cond-mat.mes-hall].
- [26] H. K. Pal and D. L. Maslov, Necessary and sufficient condition for longitudinal magnetoresistance, *Phys. Rev. B* **81**, 214438 (2010).
- [27] X.-L. Qi and S.-C. Zhang, Topological insulators and superconductors, *Rev. Mod. Phys.* **83**, 1057 (2011).
- [28] N. P. Armitage, E. J. Mele, and A. Vishwanath, Weyl and Dirac semimetals in three-dimensional solids, *Rev. Mod. Phys.* **90**, 015001 (2018).
- [29] B. Q. Lv, T. Qian, and H. Ding, Experimental perspective on three-dimensional topological semimetals, *Rev. Mod. Phys.* **93**, 025002 (2021).
- [30] B. Bradlyn, J. Cano, Z. Wang, M. G. Vergniory, C. Felser, R. J. Cava, and B. A. Bernevig, Beyond Dirac and Weyl fermions: Unconventional quasiparticles in conventional crystals, *Science* **353**, aaf5037 (2016).
- [31] Z. Zhu, G. W. Winkler, Q. Wu, J. Li, and A. A. Soluyanov, Triple point topological metals, *Phys. Rev. X* **6**, 031003 (2016).
- [32] H. Weng, C. Fang, Z. Fang, and X. Dai, Topological semimetals with triply degenerate nodal points in θ -phase tantalum nitride, *Phys. Rev. B* **93**, 241202 (2016).
- [33] W. Wu, Y. Liu, S. Li, C. Zhong, Z.-M. Yu, X.-L. Sheng, Y. X. Zhao, and S. A. Yang, Nodal surface semimetals: Theory and material realization, *Phys. Rev. B* **97**, 115125 (2018).
- [34] C. Fang, H. Weng, X. Dai, and Z. Fang, Topological nodal line semimetals, *Chinese Physics B* **25**, 117106 (2016).
- [35] Z.-M. Yu, Z. Zhang, G.-B. Liu, W. Wu, X.-P. Li, R.-W. Zhang, S. A. Yang, and Y. Yao, Encyclopedia of emergent particles in three-dimensional crystals, *Science Bulletin* **67**, 375 (2022).
- [36] X. Wang, F. Zhou, Z. Zhang, Z.-M. Yu, and Y. Yao, Hourglass charge-three Weyl phonons, *Phys. Rev. B* **106**, 214309 (2022).
- [37] R.-W. Zhang, X. Zhou, Z. Zhang, D.-S. Ma, W. Yu, Zhi and Feng, and Y. Yao, Weyl monolayer semi-half-metal and tunable anomalous Hall effect, *Nano Letters* **21**, 8749 (2021).
- [38] X. Wang, F. Zhou, Z. Zhang, W. Wu, Z.-M. Yu, and S. A. Yang, Single pair of multi-Weyl points in nonmagnetic crystals, *Phys. Rev. B* **106**, 195129 (2022).
- [39] Z.-M. Yu, Y. Yao, and S. A. Yang, Predicted unusual magnetoresistance in type-II Weyl semimetals, *Phys. Rev. Lett.* **117**, 077202 (2016).

- [40] Y. Liu, Z.-M. Yu, C. Xiao, and S. A. Yang, Quantized circulation of anomalous shift in interface reflection, *Phys. Rev. Lett.* **125**, 076801 (2020).
- [41] G. Chang, S.-Y. Xu, B. J. Wieder, D. S. Sanchez, S.-M. Huang, I. Belopolski, T.-R. Chang, S. Zhang, A. Bansil, H. Lin, and M. Z. Hasan, Unconventional chiral fermions and large topological Fermi arcs in RhSi, *Phys. Rev. Lett.* **119**, 206401 (2017).
- [42] J. Ahn, G.-Y. Guo, and N. Nagaosa, Low-frequency divergence and quantum geometry of the bulk photovoltaic effect in topological semimetals, *Phys. Rev. X* **10**, 041041 (2020).
- [43] X. Zhang, Z.-M. Yu, Y. Lu, X.-L. Sheng, H. Y. Yang, and S. A. Yang, Hybrid nodal loop metal: Unconventional magnetoresistance and material realization, *Phys. Rev. B* **97**, 125143 (2018).
- [44] N.-N. Zhao, K. Liu, and Z.-Y. Lu, Large anomalous Hall effect induced by gapped nodal lines in GdZn and GdCd, *Phys. Rev. B* **103**, 205104 (2021).
- [45] X. Dai, Z. Z. Du, and H.-Z. Lu, Negative magnetoresistance without chiral anomaly in topological insulators, *Phys. Rev. Lett.* **119**, 166601 (2017).
- [46] P. Liu, C. Cui, X.-P. Li, Z.-M. Yu, and Y. Yao, Landau level spectrum and magneto-optical conductivity in tilted Weyl semimetal, *Phys. Rev. B* **107**, 085146 (2023).
- [47] C. Zeng, X.-Q. Yu, Z.-M. Yu, and Y. Yao, Band tilt induced nonlinear Nernst effect in topological insulators: An efficient generation of high-performance spin polarization, *Phys. Rev. B* **106**, L081121 (2022).
- [48] Z. Zhu, H. Liu, Y. Ge, Z. Zhang, W. Wu, C. Xiao, and S. A. Yang, [Third-order charge transport in a magnetic topological semimetal](#) (2022), [arXiv:2209.05736 \[cond-mat.mtrl-sci\]](#).
- [49] H. Liu, J. Zhao, Y.-X. Huang, X. Feng, C. Xiao, W. Wu, S. Lai, W.-b. Gao, and S. A. Yang, Berry connection polarizability tensor and third-order Hall effect, *Phys. Rev. B* **105**, 045118 (2022).
- [50] H. Liu, J. Zhao, Y.-X. Huang, W. Wu, X.-L. Sheng, C. Xiao, and S. A. Yang, Intrinsic second-order anomalous Hall effect and its application in compensated antiferromagnets, *Phys. Rev. Lett.* **127**, 277202 (2021).
- [51] S. Nandy, G. Sharma, A. Taraphder, and S. Tewari, Chiral anomaly as the origin of the planar Hall effect in Weyl semimetals, *Phys. Rev. Lett.* **119**, 176804 (2017).
- [52] M.-X. Deng, Y.-Y. Yang, W. Luo, R. Ma, C.-Y. Zhu, R.-Q. Wang, L. Sheng, and D. Y. Xing, Positive longitudinal spin magnetoconductivity in \mathbb{Z}_2 topological dirac semimetals, *Phys. Rev. B* **100**, 235105 (2019).
- [53] A. Yamada and Y. Fuseya, Negative magnetoresistance and sign change of the planar Hall effect due to negative off-diagonal effective mass in Weyl semimetals, *Phys. Rev. B* **105**, 205207 (2022).
- [54] M.-X. Deng, H.-J. Duan, W. Luo, W. Y. Deng, R.-Q. Wang, and L. Sheng, Quantum oscillation modulated angular dependence of the positive longitudinal magnetoconductivity and planar Hall effect in Weyl semimetals, *Phys. Rev. B* **99**, 165146 (2019).
- [55] M.-X. Deng, Y.-C. Hu, W. Luo, H.-J. Duan, and R.-Q. Wang, Connection between topological pumping effect and chiral anomaly in Weyl semimetals, *Phys. Rev. B* **106**, 075139 (2022).
- [56] D. Ma, H. Jiang, H. Liu, and X. C. Xie, Planar Hall effect in tilted Weyl semimetals, *Phys. Rev. B* **99**, 115121 (2019).
- [57] M. Imran and S. Hershfield, Berry curvature force and Lorentz force comparison in the magnetotransport of Weyl semimetals, *Phys. Rev. B* **98**, 205139 (2018).
- [58] S. Woo, B. Min, and H. Min, Semiclassical magnetotransport including effects of Berry curvature and Lorentz force, *Phys. Rev. B* **105**, 205126 (2022).
- [59] Sonika, M. K. Hooda, S. Sharma, and C. S. Yadav, Planar Hall effect in Cu intercalated PdTe₂, [arXiv:2110.14251](#) (2021), [arXiv:2110.14251 \[cond-mat.str-el\]](#).
- [60] J. Ge, D. Ma, Y. Liu, H. Wang, Y. Li, J. Luo, T. Luo, Y. Xing, J. Yan, D. Mandrus, H. Liu, X. C. Xie, and J. Wang, Unconventional Hall effect induced by Berry curvature, *National Science Review* **7**, 1879 (2020).
- [61] Q. Liu, F. Fei, B. Chen, X. Bo, B. Wei, S. Zhang, M. Zhang, F. Xie, M. Naveed, X. Wan, F. Song, and B. Wang, Nontopological origin of the planar Hall effect in the type-II Dirac semimetal NiTe₂, *Phys. Rev. B* **99**, 155119 (2019).
- [62] P. Li, C. Zhang, Y. Wen, L. Cheng, G. Nichols, D. G. Cory, G.-X. Miao, and X.-X. Zhang, Anisotropic planar Hall effect in the type-II topological Weyl semimetal WTe₂, *Phys. Rev. B* **100**, 205128 (2019).
- [63] S. Xu, H. Wang, X.-Y. Wang, Y. Su, P. Cheng, and T.-L. Xia, Planar Hall effect in the Dirac semimetal PdTe₂, [arXiv e-prints](#) , [arXiv:1811.06767](#) (2018), [arXiv:1811.06767 \[cond-mat.mtrl-sci\]](#).
- [64] M. Wu, G. Zheng, W. Chu, Y. Liu, W. Gao, H. Zhang, J. Lu, Y. Han, J. Zhou, W. Ning, and M. Tian, Probing the chiral anomaly by planar Hall effect in Dirac semimetal Cd₃As₂ nanoplates, *Phys. Rev. B* **98**, 161110 (2018).
- [65] Y. J. Wang, J. X. Gong, D. D. Liang, M. Ge, J. R. Wang, W. K. Zhu, and C. J. Zhang, Planar Hall effect in type-II Weyl semimetal WTe₂, [arXiv e-prints](#) , [arXiv:1801.05929](#) (2018), [arXiv:1801.05929 \[cond-mat.mtrl-sci\]](#).
- [66] R. Singha, S. Roy, A. Pariari, B. Satpati, and P. Mandal, Planar Hall effect in the type-II Dirac semimetal VAl₃, *Phys. Rev. B* **98**, 081103 (2018).
- [67] S. Liang, J. Lin, S. Kushwaha, J. Xing, N. Ni, R. J. Cava, and N. P. Ong, Experimental tests of the chiral anomaly magnetoresistance in the Dirac-Weyl semimetals Na₃Bi and GdPtBi, *Phys. Rev. X* **8**, 031002 (2018).
- [68] N. Kumar, S. N. Guin, C. Felser, and C. Shekhar, Planar Hall effect in the Weyl semimetal GdPtBi, *Phys. Rev. B* **98**, 041103 (2018).
- [69] Sonika, S. Gagwar, and C. S. Yadav, [Planar Hall effect, anisotropic magnetoresistance and thermal transport studies of Ag doped PdTe₂](#) (2023), [arXiv:2303.18075 \[cond-mat.str-el\]](#).
- [70] L. Li, E. Yi, B. Wang, G. Yu, B. Shen, Z. Yan, and M. Wang, Higher-order oscillatory planar Hall effect in topological kagome metal, *npj Quantum Materials* **8**, 2 (2023).
- [71] J. Zhong, J. Zhuang, and Y. Du, Recent progress on the planar hall effect in quantum materials, *Chinese Physics B* **32**, 047203 (2023).
- [72] G. Sharma, S. Nandy, and S. Tewari, Sign of longitudinal magnetoconductivity and the planar Hall effect in Weyl semimetals, *Phys. Rev. B* **102**, 205107 (2020).
- [73] S. Yadav, S. Fazzini, and I. Mandal, Magneto-transport signatures in periodically-driven Weyl and multi-Weyl semimetals, *Physica E: Low-dimensional Systems and Nanostructures* **144**, 115444 (2022).

- [74] F. Abdulla, A. Das, S. Rao, and G. Murthy, Time-reversal-broken Weyl semimetal in the Hofstadter regime, *SciPost Phys. Core* **5**, 014 (2022).
- [75] B. Sadhukhan and T. Nag, Effect of chirality imbalance on Hall transport of PrRhC₂, *Phys. Rev. B* **107**, L081110 (2023).
- [76] S. Nandy, A. Taraphder, and S. Tewari, Berry phase theory of planar Hall effect in topological insulators, *Scientific Reports* **8**, 1 (2018).
- [77] A. Taskin, H. F. Legg, F. Yang, S. Sasaki, Y. Kanai, K. Matsumoto, A. Rosch, and Y. Ando, Planar Hall effect from the surface of topological insulators, *Nature communications* **8**, 1 (2017).
- [78] P. Wang, T. Hou, F. Tang, P. Wang, Y. Han, Y. Ren, H. Zeng, L. Zhang, and Z. Qiao, Temperature dependent in-plane anisotropic magnetoresistance in HfTe₅ thin layers, *Chinese Physics Letters* **38**, 017201 (2021).
- [79] N. Nagaosa, J. Sinova, S. Onoda, A. H. MacDonald, and N. P. Ong, Anomalous Hall effect, *Rev. Mod. Phys.* **82**, 1539 (2010).
- [80] D. Xiao, J. Shi, and Q. Niu, Berry phase correction to electron density of states in solids, *Phys. Rev. Lett.* **95**, 137204 (2005).
- [81] S. J. Watzman, T. M. McCormick, C. Shekhar, S.-C. Wu, Y. Sun, A. Prakash, C. Felser, N. Trivedi, and J. P. Heremans, Dirac dispersion generates unusually large Nernst effect in Weyl semimetals, *Phys. Rev. B* **97**, 161404 (2018).
- [82] C. Shekhar, A. K. Nayak, Y. Sun, M. Schmidt, M. Nicklas, I. Leermakers, U. Zeitler, Y. Skourski, J. Wosnitza, Z. Liu, *et al.*, Extremely large magnetoresistance and ultrahigh mobility in the topological Weyl semimetal candidate NbP, *Nature Physics* **11**, 645 (2015).
- [83] M. Naumann, F. Arnold, M. D. Bachmann, K. A. Modic, P. J. W. Moll, V. Süß, M. Schmidt, and E. Hassinger, Orbital effect and weak localization in the longitudinal magnetoresistance of weyl semimetals NbP, NbAs, TaP, and TaAs, *Phys. Rev. Mater.* **4**, 034201 (2020).
- [84] J. Cao, C. Zeng, X.-P. Li, M. Wang, S. A. Yang, Z.-M. Yu, and Y. Yao, Low-frequency divergence of circular photomagnetic effect in topological semimetals (2022), [arXiv:2201.06243 \[cond-mat.mes-hall\]](https://arxiv.org/abs/2201.06243).
- [85] A. A. Burkov, M. D. Hook, and L. Balents, Topological nodal semimetals, *Phys. Rev. B* **84**, 235126 (2011).
- [86] H. Weng, Y. Liang, Q. Xu, R. Yu, Z. Fang, X. Dai, and Y. Kawazoe, Topological node-line semimetal in three-dimensional graphene networks, *Phys. Rev. B* **92**, 045108 (2015).
- [87] R. Yu, H. Weng, Z. Fang, X. Dai, and X. Hu, Topological node-line semimetal and Dirac semimetal state in antiperovskite Cu₃PdN, *Phys. Rev. Lett.* **115**, 036807 (2015).
- [88] C. Fang, H. Weng, X. Dai, and Z. Fang, Topological nodal line semimetals, *Chinese Physics B* **25**, 117106 (2016).
- [89] S. Li, Z.-M. Yu, Y. Liu, S. Guan, S.-S. Wang, X. Zhang, Y. Yao, and S. A. Yang, Type-II nodal loops: Theory and material realization, *Phys. Rev. B* **96**, 081106 (2017).
- [90] S. Li, Y. Liu, B. Fu, Z.-M. Yu, S. A. Yang, and Y. Yao, Almost ideal nodal-loop semimetal in monoclinic CuTeO₃ material, *Phys. Rev. B* **97**, 245148 (2018).
- [91] T. Liang, J. Lin, Q. Gibson, S. Kushwaha, M. Liu, W. Wang, H. Xiong, J. A. Sobota, M. Hashimoto, P. S. Kirchmann, Z.-X. Shen, R. J. Cava, and N. P. Ong, Anomalous Hall effect in ZrTe₅, *Nature Physics* **14**, 451 (2018).
- [92] J. Zhou, W. Zhang, Y. C. Lin, J. Cao, Y. Zhou, W. Jiang, H. Du, B. Tang, J. Shi, B. Jiang, X. Cao, B. Lin, Q. Fu, C. Zhu, W. Guo, Y. Huang, Y. Yao, S. S. P. Parkin, J. Zhou, Y. Gao, Y. Wang, Y. Hou, Y. Yao, K. Suenaga, X. Wu, and Z. Liu, Heterodimensional superlattice with in-plane anomalous Hall effect, *Nature* **609**, 46 (2022).
- [93] Z.-M. Yu, W. Wu, Y. X. Zhao, and S. A. Yang, Circumventing the no-go theorem: A single Weyl point without surface Fermi arcs, *Phys. Rev. B* **100**, 041118 (2019).
- [94] M. Xiao, L. Ye, C. Qiu, H. He, Z. Liu, and S. Fan, Experimental demonstration of acoustic semimetal with topologically charged nodal surface, *Science Advances* **6**, eaav2360 (2020).